LETTERS

Kinase-regulated quantal assemblies and kiss-and-run recycling of caveolae

Lucas Pelkmans[1] & Marino Zerial[1]

A functional genomics approach has revealed that caveolae/raft-mediated endocytosis is subject to regulation by a large number of kinases[1]. Here we explore the role of some of these kinases in caveolae dynamics. We discover that caveolae operate using principles different from classical membrane trafficking. First, each caveolar coat contains a set number (one 'quantum') of caveolin-1 molecules. Second, caveolae are either stored as in stationary multi-caveolar structures at the plasma membrane, or undergo continuous cycles of fission and fusion with the plasma membrane in a small volume beneath the surface, without disassembling the caveolar coat. Third, a switch mechanism shifts caveolae from this localized cycle to long-range cytoplasmic transport. We have identified six kinases that regulate different steps of the caveolar cycle. Our observations reveal new principles in caveolae trafficking and suggest that the dynamic properties of caveolae and their transport competence are regulated by different kinases operating at several levels.

Caveolae are involved in dynamic cellular processes such as signal transduction[2] and endocytosis[3], but appear to be constitutively immobile[4,5]. Inside the cell, caveolar vesicles dock on, fuse with and are released from endocytic organelles without disassembling the caveolin-1 (CAV1) coat[6]. It is not known whether caveolae are assembled *de novo* at the cell surface or originate from intracellular pools, whether they interact dynamically with the plasma membrane, how they participate in membrane trafficking and how this is regulated by kinases[1]. We address these questions using a combination of quantitative total internal reflection fluorescence microscopy (TIR-FM)[7], computational analysis and functional genomics using RNA interference (RNAi)[1].

Caveolae were visualized in HeLa cells stably expressing CAV1 labelled with green fluorescent protein (GFP)[6] (see Supplementary Information for detailed methods). Fitting the intensity distributions of the visualized spots to multiple gaussian curves revealed that caveolar structures were assembled from unit-sized building blocks, with a constant fluorescence intensity quantum (q). (Fig. 1a, b). Quantal incorporation into synaptic vesicles has been shown for neurotransmitters and lipid dyes[8,9]. To assign each gaussian peak to a morphologically known structure, we estimated their size. CAV1–GFP spot sizes of $q_{n<4}$ were as large as the diffraction limit of our imaging system (~200 nm) (Supplementary Fig. S1a–c), but size differences became apparent for higher q values ($q_{\geq 4}$). Together with previous ultrastructural analysis of CAV1–GFP on the cell surface[5,10], we conclude that the q_1 structures (~50 nm in size) are individual caveolae, and that $q_{>1}$ structures are grape-like clusters of multiple caveolae.

Using mouse *Cav1*$^{-/-}$ fibroblasts[11] expressing CAV1–GFP, the number of CAV1 molecules in q_1 structures was estimated to be 144 ± 39 (Supplementary Fig. S1). The intensity of CAV1–GFP q_1 quanta in HeLa cells was ~0.56 of that in *Cav1*$^{-/-}$ fibroblasts (Fig. 1b and Supplementary Fig. S1f). As CAV1–GFP is expressed at similar levels as endogenous CAV1 in HeLa cells[6], this indicates that quanta of both cell lines contain a similar number of CAV1 molecules, and that the GFP moiety does not disturb incorporation or quantal assembly. The number of CAV1 molecules in quanta was independent of expression level (Supplementary Fig. S1d, f). However, upon 5–10-fold overexpression of CAV1–GFP, CAV1 also appeared in surface structures at sub-quantal intensity (0.1–0.3q; Supplementary Fig. S1e, f) that, in contrast to individual caveolae, showed lateral mobility within the plane of the membrane (Supplementary Video 1). These might represent CAV1 oligomers that failed to be incorporated into caveolae owing to saturation of the assembly mechanism.

We observed that many caveolae are not fixed at the plasma membrane, but instead appear and disappear (Supplementary Videos 2, 2a), as indicated by rapid quantal increases and complete losses of fluorescence intensity (Fig. 1c, d and Supplementary Videos 3, 3a, 3b). During docking, spot intensity remained constant and CAV1–GFP did not diffuse into the surrounding membrane (Supplementary Fig. S1i), suggesting that pre-assembled caveolar vesicles keep their structural integrity while cycling between the cytoplasm and the cell surface[6].

Most structures showing kiss-and-run interactions (90/398) were individual caveolae (Fig. 1d). In fact, over a period of 300 s, 45% (71/158) of all individual caveolae were dynamic. Occasionally, we observed the docking of a q_1 vesicle and the subsequent docking of a second q_1 vesicle, resulting in the formation of a q_2 structure (Supplementary Fig. S1j). We thus conclude that multi-caveolar assemblies are formed by multiple individual caveolar vesicles docking on top of one another. These are stably attached to the cell surface, whereas half of the individual caveolae show continuous kiss-and-run interactions with the plasma membrane.

To demonstrate that caveolae can undergo a cycle of docking, fusion and fission, we used pH quenching[12] with dual colour TIR-FM. The outside of caveolar vesicles was visualized with CAV1 tagged with monomeric red fluorescent protein (CAV1–mRFP) and the vesicle lumen was visualized with fluorescein-isothiocyanate-labelled Cholera toxin B (FITC-ChTxB)[13]. Because the interior of caveolar vesicles and caveosomes is pH neutral[14], we used rapid loss of FITC signal upon acidification as the readout for fusion.

Using TIR-FM, we found that most caveolar structures incorporated the FITC-ChTxB toxin, including those showing kiss-and-run interactions with the plasma membrane (Supplementary Fig. S2a and Supplementary Video 4). Upon acidification of the extracellular medium to pH 5.5, the FITC signal was quenched, predominantly in multi-caveolar assemblies; it was not quenched in several individual caveolae, suggesting that these caveolae were docked on, but not continuous with the plasma membrane (Fig. 1e). However, the FITC signal was rapidly quenched to background levels in these structures about 1 s after docking (Fig. 1f, g, Supplementary Fig. S2b and Supplementary Videos 4a–c). Similar quenching kinetics were observed at an extracellular pH of 6.2, a pH at which some signal

[1]Max Planck Institute for Molecular Cell Biology and Genetics, Pfotenhauerstrasse 108, 01307 Dresden, Germany.

remained (in agreement with the pK_a of FITC) (Fig. 1g). Out of 32 docking vesicles, 27 became rapidly quenched in a *N*-ethylmaleimide (NEM)-sensitive manner (Supplementary Fig. S2b, d). Addition of ionophores, which equilibrate protons across membranes, resulted in quenched FITC signal in docking caveolar vesicles (Supplementary Fig. S2b). Together, these observations indicate that intracellular caveolar vesicles that have incorporated ChTxB during a previous visit to the cell surface or to intracellular, pH-neutral organelles like caveosomes[6,14], can dock at and fuse with the plasma membrane. Alternatively, model membrane experiments suggest that exposure of the vesicle lumen to the extracellular medium during kiss-and-run interactions might be determined by length-controlled accessibility of a tubular membranous neck continuously connected to the surface[15].

Under conditions of neutral extracellular pH, FITC-ChTxB was not released into the surrounding membrane after fusion of a caveolar vesicle. However, release did occur when the glycosphingolipid-bound toxin was exocytosed by other, CAV1–mRFP-negative vesicles (Fig. 1f and Supplementary Fig. S2c), in a manner similar to the release of lipid dyes or transmembrane proteins from secretory

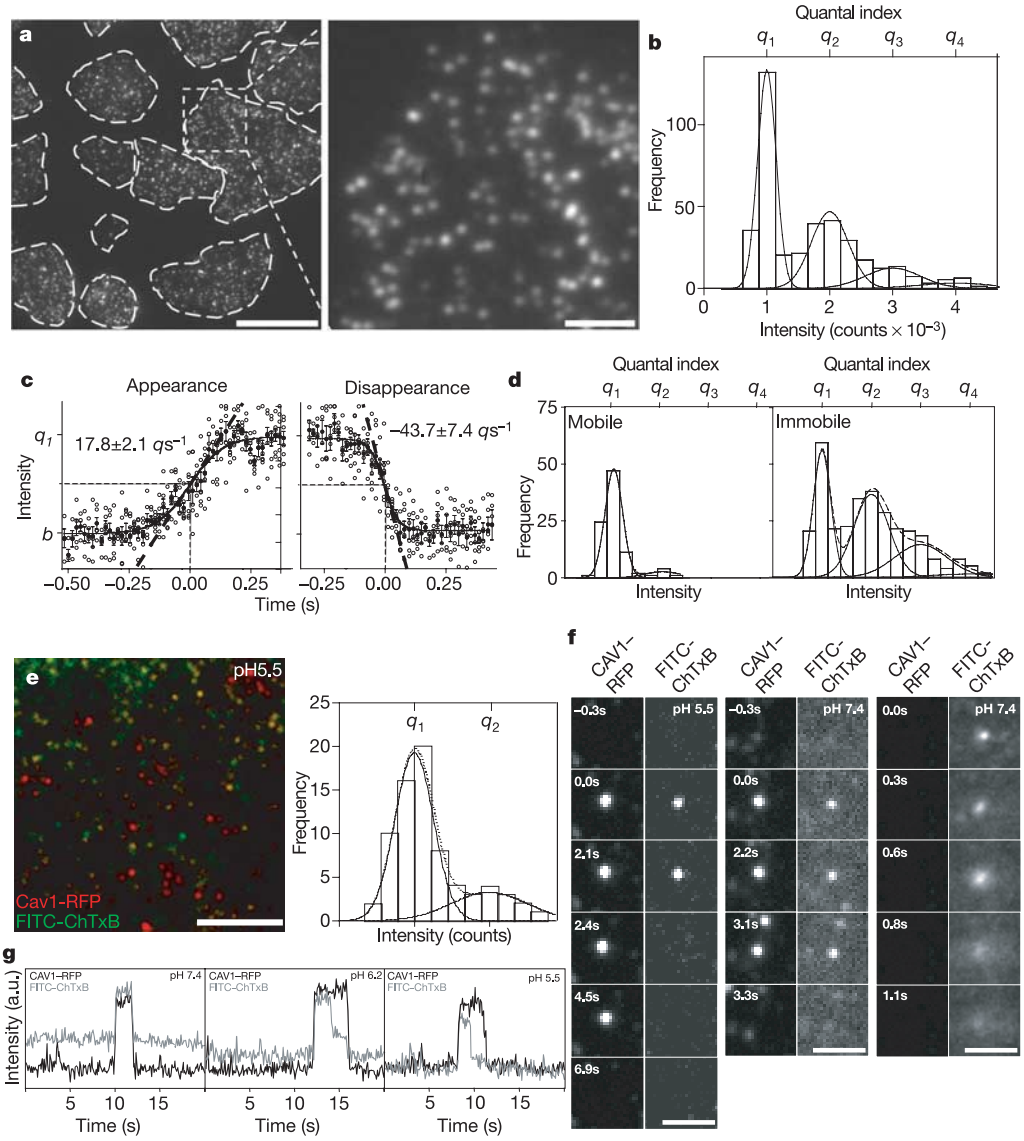

Figure 1 | Quantal assembly and kiss-and-run of caveolar structures. **a**, TIR-FM of HeLa cells stably expressing CAV1–GFP. Scale bars, 10 μm (left) and 2 μm (right). **b**, Intensity histogram of 396 CAV1–GFP-positive structures in HeLa cells, fitted to 4 gaussian curves (degrees of freedom (d.f.) = 13; $R^2 = 0.99$; absolute sum of squares (S.S.) = 154.8; residuals ($S_{y.x}$) = 3.45). The mean of the first peak is defined as *q*. **c**, Plots of intensity over time (17-ms interval) of 12 appearing and 10 disappearing structures in TIR-FM, and sigmoidal curve fits (solid lines) of average (±s.e.m.) values (filled circles) (appearing: d.f. = 344, $R^2 = 0.82$, S.S. = 1.7, $S_{y.x} = 0.07$; disappearing: d.f. = 233, $R^2 = 0.81$, S.S. = 1.3, $S_{y.x} = 0.07$). The rates of appearance ($17.8 \pm 2.1\, q\, s^{-1}$) and disappearance ($-43.7 \pm 7.4\, q\, s^{-1}$) and the level of background signal (*b*) are shown on the graph. **d**, Intensity histograms and gaussian fits of 90 docking/mobile (d.f. = 6, $R^2 = 1.00$, S.S. = 4.8, $S_{y.x} = 0.89$) and 308 fixed/immobile structures (d.f. = 14, $R^2 = 0.97$, S.S. = 146.3, $S_{y.x} = 3.23$). Of the 90 mobile spots, 71 are q_1 and 7 are q_2. Of the 308 fixed spots, 87 are q_1 and 221 are $q_{n>1}$. **e**, Dual-colour TIR-FM, intensity histogram and gaussian fit of 73 caveolar structures with non-quenchable FITC-ChTxB (d.f. = 10, $R^2 = 0.97$, S.S. = 12.9, $S_{y.x} = 1.14$). Scale bar, 5 μm. **f**, Selected frames from 100-ms interval recordings. Left, FITC-ChTxB in a caveolar vesicle, quenched by low extracellular pH during docking. Middle, FITC-ChTxB in a caveolar vesicle remains sequestered at neutral pH during docking. Right, FITC-ChTxB in a non-caveolar vesicle is released into the surrounding membrane at neutral pH during docking. Scale bar, 1 μm. **g**, CAV1–RFP and FITC-ChTxB fluorescence intensity traces (100-ms intervals; no background correction) during kiss-and-run of an individual caveola at extracellular pH 7.4, 6.2 or 5.5. Fusion is detected as as rapid quenching of the FITC signal before the RFP signal disappears.

vesicles[16]. Thus, during the fusion of individual caveolae with the plasma membrane, the caveolar coat does not fully dissociate, and it retains the ability to sequester a ganglioside GM1-associated multivalent ligand, similar to intracellular caveolar vesicles[6].

To follow the origin and fate of the cycling population of caveolar vesicles, we combined TIR-FM with epifluorescence microscopy (Epi-FM)[16]. A spot appearing in TIR-FM was invariably observed first in Epi-FM (Fig. 2a, c and Supplementary Videos 5, 5a), confirming that caveolae are not assembled *de novo* at the surface, but instead are pre-assembled in intracellular caveolar vesicle stores and then transported to the cell surface. Indeed, we could directly monitor a FITC-ChTxB-containing, pre-existing vesicle appearing from the cytoplasm, docking on the surface, exposing its lumen to the extracellular space, and internalizing again (Supplementary Fig. S3). Between docking events, we occasionally observed rapid, directional movement. The majority of mobile caveolae, however, repeatedly docked in a small area of the plasma membrane, and combined this with short-range motility below the surface (Fig. 2b and Supplementary Video 5b). We performed statistical analysis of the spatial distribution of all docking events over a 300-s recording period, and confirmed that most were confined to an area of 3–8 μm^2 (Fig. 2d). Apparently individual caveolae undergo (1) continuous short-range cycles of fusion and internalization, during which they do not travel long distances but are restricted within a small cytoplasmic volume beneath the cell surface, and (2) occasional trafficking between the plasma membrane and intracellular pools. This is consistent with a slow exchange between these two pools and a seemingly fixed position of caveolar structures on the cell surface[4,5].

We next performed an in-depth analysis of six kinases identified as potential candidate regulators of caveolae/raft-mediated endocytosis that are also involved in infectious entry of simian virus 40 (SV40)[1]. A series of RNAi phenotypes reflected functions at distinct steps of the caveolar cycle described above. First, the silencing of *ARAF1* (also known as *ARAF*), a serine/threonine kinase involved in mitogenic signalling, resulted in diffuse CAV1–GFP staining that was laterally mobile, in addition to the characteristic spot-like pattern (Fig. 3a, Supplementary Fig. S2c and Supplementary Video 6). We suggest that in the absence of *ARAF1*, the caveolar coat is less stable or inefficiently assembled.

Second, ablation of *MGC26597* (a hypothetical kinase with a

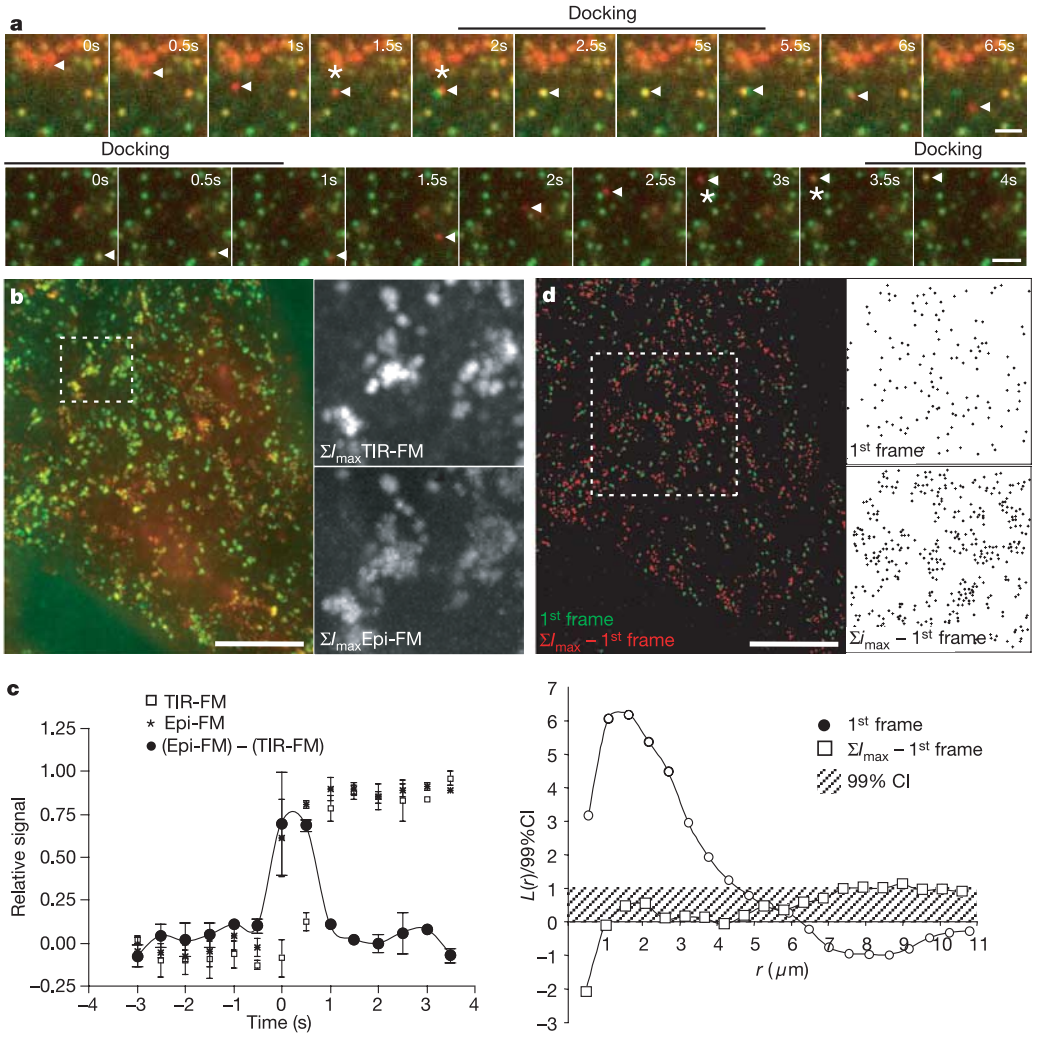

Figure 2 | Cycling is restricted to local areas beneath the plasma membrane. **a**, Combined TIR-FM (green) and Epi-FM (red). Plasma membrane kiss-and-run by a caveolar vesicle departing from an intracellular organelle (top) and rapid, directional transport of a caveolar vesicle between two docking events (bottom). Time is relative to the first frame. Scale bars, 1 μm (top), 2 μm (bottom). **b**, Maximum intensity projections (ΣI_{max}) of TIR-FM (green) and Epi-FM (red) time-lapse sequence reveal areas of clustered spots that co-localize with each other. Scale bar, 10 μm. **c**, Average (±s.e.m.) relative intensities of docking sites measured by TIR-FM (open squares) and Epi-FM (stars). The Epi-FM signal appears 1–2 frames (500–1,000 ms) before the TIR-FM signal (see asterisks in **a**). **d**, Quantification of clustering of docking events by coordinate determination and, Ripley's *K* function analysis of caveolar structures on the surface (at the first frame, green) and of docking events during time-lapse (ΣI_{max} minus the first frame, red). Scale bar, 10 μm.

phosphoinositide 4-phosphate 5-kinase (PI(4)P5K) homology domain) or *SRC* resulted in clustering of caveolae (Fig. 3a), leading to an increase in multi-caveolar assemblies ($q_{n>3}$) at the expense of individual caveolae. As a result, caveolar structures accumulated at the cell surface, and both the dynamics of caveolae (Fig. 3b, c) and the internalization of SV40 particles were strongly reduced (Supplementary Fig. S2d and Supplementary Video 7).

Third, silencing of two serine/threonine kinases (*KIAA0999* and *MAP3K2*), strongly reduced kiss-and-run dynamics, leading to an accumulation of caveolar structures at the cell surface (Fig. 3b, c and Supplementary Video 8) without affecting caveolae coat assembly or clustering (not shown). Conversely, knockdown of the Ser/Thr MAPK-related kinase *DYRK3* strongly increased the dynamics of caveolar vesicles (Fig. 3b, c) and had a minor destabilizing effect on the caveolar coat (Supplementary Video 9).

Increased dynamics were also observed upon exposure to okadaic acid or SV40, both known to stimulate caveolae-mediated endocytosis[4,17] (Fig. 3b, c and Supplementary Video 10). There was no net change in the number of caveolae at the cell surface, but we did detect a three- to fivefold increase in the number of docking events, which occurred at random positions on the plasma membrane (Fig. 3c, d), Random docking is also seen after actin depolymerization (data not shown), and this is initiated by SV40 (ref. 4). Because cell-surface and intracellular pools of CAV1 exchange upon addition of okadaic acid[5] or SV40 (data not shown), we propose that stimulation of caveolae-mediated endocytosis requires elimination

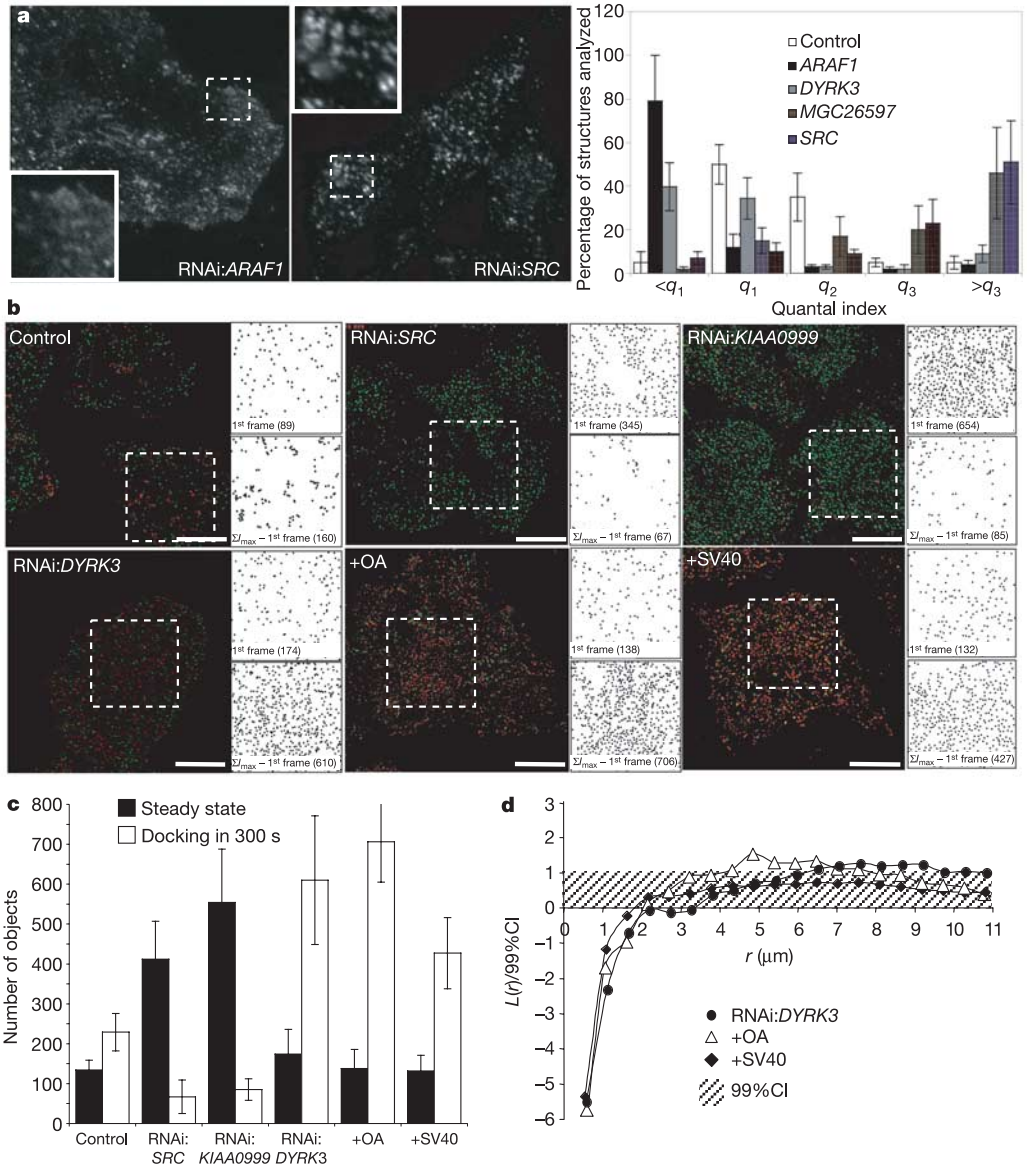

Figure 3 | Caveolae coat stability, clustering and cycling mode are controlled by kinases. a, TIR-FM and quantal index analysis (average values ± s.e.m.; $n = 212–479$; 3 cells) of CAV1–GFP shows that RNAi-mediated knockdown of *ARAF1* (RNAi:*ARAF1*) results in diffuse staining ($<q_1$) and RNAi:*SRC* results in the formation of large, multi-caveolar clusters. **b**, Coordinate determination of caveolar docking sites during RNAi-mediated knockdown of *SRC*, *KIAA0999* or *DYRK3*, and after treatment with 1 μM okadaic acid (OA) or exposure to SV40. Scale bars, 10 μm. **c**, Average CAV1–GFP spot density (±s.e.m.) determined for the first frame and ΣI_{max} minus the first frame, from 8 areas of 21.6 μm^2 each. RNAi:*SRC* and RNAi:*KIAA0999* reduce the number of docking events and increase the number of caveolar structures on the cell surface. RNAi:*DYRK3*, OA-treatment and SV40 incubation increase the number of docking events. **d**, Quantification of clustering of docking events after RNAi:*DYRK3*, OA-treatment and SV40 exposure shows loss of clustering. Regions of the curve above the 99% CI indicate clusters of caveolae within an area size of radius *r* (see Methods).

of the spatial restrictions on caveolae dynamics imposed by the actin cytoskeleton[4], resulting in a switch from futile kiss-and-run cycles to long-range, microtubule-dependent transport cycles. This results in 'committed' internalization of caveolae to intracellular organelles and their replenishment with caveolar vesicles from intracellular locations.

In this study, we have identified new principles of caveolae membrane trafficking. First, a quantal number of 144 ± 39 molecules of CAV1 are incorporated in one caveolar coat. Second, whereas caveolae not engaged in trafficking are stored as clusters in multi-caveolar assemblies that communicate with the extracellular space, transport-competent caveolae undergo constitutive kiss-and-run cycles in a small volume underneath the plasma membrane, during which the caveolar coat stays intact and sequesters multivalent, sphingolipid-bound cargo. Third, a molecular switch changes the mode of cycling from short- to long-range and activates caveolae-mediated transport to intracellular locations (such as caveosomes[14] and, to a lesser extent, early endosomes[6]). Intracellular caveolar vesicles are concomitantly recycled to the plasma membrane.

We have identified six kinases that regulate coat stability (*ARAF1*), caveolae clustering (*SRC*, *MGC26597*), kiss-and-run dynamics (*KIAA0999*, *MAP3K2*) and long-range cycling (*DYRK3*). Mitogenic signalling downstream of *ARAF1* might act through (de)stabilizing the caveolar signalling scaffold[2] and differentially shaping CAV1–GFP-positive membranes[1].

Ablation of *SRC* or *MGC26597* causes the same caveolae-clustering phenotype as overexpression of the GTP hydrolysis-deficient mutant of dynamin2 (ref. 18; Supplementary Fig. S2e), and blocks infectious entry of SV40. This is consistent with suggested roles for *SRC* in caveolae function and/or dynamics[19,20]. The specific recruitment and activation of dynamin2 on caveolar structures might be regulated by *MGC26597* (through phosphatidylinositol-4,5-bisphosphate ($PtdIns(4,5)P_2$) synthesis; ref. 21) and *SRC*[22]. *MGC26597* could be a caveolae/lipid raft-mediated endocytosis-specific PI(4)P5K, as it is not required for clathrin-mediated endocytosis[1].

Differential regulation of short- and long-distance cycling between the cell surface and intracellular organelles by *KIAA0999*, *MAP3K2* and *DYRK3* points to the existence of kinase-regulated molecular machinery that can activate these two modes of trafficking and switch between them. This probably involves changes in the cortical actin cytoskeleton and activation of microtubule-dependent motility[1,10,23].

Finally, we can make suggestions regarding different modes of caveolae- and raft-dependent endocytosis. First, a ligand-activated switch from short- to long-range cycles induces committed internalization of caveolae. Second, directional transport independent of this switch might be established when locally cycling caveolae transiently fuse with nearby organelles when a cue induces ligand release[6]. Third, a mechanism might be in place to destabilize the caveolar coat at the plasma membrane, allowing release of lipid rafts and their internalization by means of non-caveolae-derived vesicles, which could be under the control of mitogenic kinases[1]. Continuing with the combined approaches of functional genomics and TIR-FM will allow systems analysis and a more detailed understanding of these related processes.

METHODS

For full details of the methods used, please refer to the Supplementary Information.

Cell culture and transfection. All cells were cultured in medium containing 10% fetal calf serum. The medium for cells expressing CAV1–GFP or CAV1–mRFP contained 500 $\mu g\,ml^{-1}$ G418. Transient transfections were performed by lipofection using FuGene6 (Roche) and short interfering RNA was transfected using Oligofectamine (Invitrogen). For imaging purposes, cells were plated in glass-bottomed micro-well dishes (MatTek) and maintained in CO_2-independent medium (GibcoBRL). Time-lapse experiments were performed at 25 °C and 37 °C.

Imaging. Imaging was performed using an Olympus IX70 inverted microscope equipped with a dual-port condensor (TILL Photonics), an argon-krypton laser (Innova 70C Spectrum, Coherent) and a 100 W mercury arc lamp light source, to allow both Epi-FM and TIR-FM. The laser beam was focused at an off-axis position in the back focal plane of high numerical aperture × 63/NA 1.45 (Olympus) or × 100/NA 1.45 (Zeiss) oil immersion objectives, such that the laser beam struck the interface between the glass and cell at an angle less than 55°. As a result, the laser light underwent total internal reflection, leading to the excitation of molecules within 100 nm above the interface only. For dual-colour experiments, a beam splitter (Dual-View Micro-Imager, Optical Insights) was used to project green and red components side by side onto a back-illuminated CCD camera (Micromax 512BFT, Roper Scientific). Time-lapse sequences were acquired at 100–500-ms intervals. For high-speed imaging (17-ms intervals), a 50 × 50 pixel region of interest was selected.

Identification of quantal assembly. Background-corrected intensity histograms were fitted to functions consisting of the sum of 2 or 4 gaussian curves:

$$F(I) = \sum_{k=1}^{k=n} v_k e^{-\frac{(I-kq)^2}{2k\sigma_v^2}} \quad (1)$$

where F is the number of caveolar structures at a given intensity I; v_k is the amplitude of the kth peak, σ_v is the variance of the intensity of an individual quantum and q is the intensity of an individual quantum. Structures with I values with >95% probability of belonging to the $k = 1$ gaussian curve (q_1 spots) were used to determine the number of CAV1–GFP molecules.

Determination of the number of incorporated caveolin-1 molecules. To calculate the number of CAV1–GFP molecules in q_1 spots, we compared the distribution of integrated gaussian curves fitted to radial sweeps of 375 rotavirus-like particles (VLPs) containing 120 molecules of GFP with the distribution of integrated gaussian curves fitted to radial sweeps of 405 q_1 spots (Supplementary Fig. S1).

Analysis of fusion events. HeLa cells expressing CAV1–mRFP were allowed to bind ~10,000 molecules of FITC-ChTxB for 5 min at 37 °C and were then extensively washed with warm CO_2-independent medium. Cells were transferred to the microscope and the imaging system was prepared to record kiss-and-run dynamics. An equal amount of citric acid-buffered, CO_2-independent medium was subsequently added to obtain a final pH of 5.5 (or 6.2) and dynamics of CAV1–mRFP and FITC-ChTxB were immediately recorded using dual-colour TIR-FM. Each video was finished within 1 min of acidification of the medium.

Statistical analysis using Ripley's *K* function. Coordinates of docking events on the plasma membrane were used to determine the distance between each docking event and to analyse the second-order property of the point pattern, defined by Ripley's K function:

$$K(r) = \frac{N(r)}{\lambda} \quad (2)$$

where $N(r)$ is the expected number of neighbours within a distance r, and $K(r)$ is $N(r)$ normalized to λ, the density of the pattern. The function used in our analysis is derived from equation (2) and describes $L(r)$, which is $K(r)$ corrected for values at complete spatial randomness (CSR) at which $N(r)$ is $\lambda\pi r^2$:

$$L(r) = \sqrt{\frac{K(r)}{\pi}} - r \quad (3)$$

At CSR, which is used as the benchmark in our analysis, $L(r)$ is 0. Monte Carlo simulations were performed to calculate the 99% confidence interval (CI) for CSR and $L(r)$ values are presented relative to the 99%CI. $L(r)$ functions were plotted and regions of the curve that emerge above the 99%CI indicate significant clustering within an area size of radius r.

Received 1 March; accepted 25 May 2005.

1. Pelkmans, L. *et al.* Genome-wide analysis of human kinases in clathrin- and caveolae/raft-mediated endocytosis. *Nature* doi:10.1038/nature03571 (this issue).
2. Razani, B., Woodman, S. E. & Lisanti, M. P. Caveolae: from cell biology to animal physiology. *Pharmacol. Rev.* **54,** 431–467 (2002).
3. Pelkmans, L. & Helenius, A. Endocytosis via caveolae. *Traffic* **3,** 311–320 (2002).
4. Pelkmans, L., Puntener, D. & Helenius, A. Local actin polymerization and dynamin recruitment in SV40-induced internalization of caveolae. *Science* **296,** 535–539 (2002).
5. Thomsen, P., Roepstorff, K., Stahlhut, M. & van Deurs, B. Caveolae are highly immobile plasma membrane microdomains, which are not involved in constitutive endocytic trafficking. *Mol. Biol. Cell* **13,** 238–250 (2002).
6. Pelkmans, L., Burli, T., Zerial, M. & Helenius, A. Caveolin-stabilized membrane domains as multifunctional transport and sorting devices in endocytic membrane traffic. *Cell* **118,** 767–780 (2004).

7. Axelrod, D., Burghardt, T. P. & Thompson, N. L. Total internal reflection fluorescence. *Annu. Rev. Biophys. Bioeng.* **13,** 247–268 (1984).
8. Katz, B. Quantal mechanism of neural transmitter release. *Science* **173,** 123–126 (1971).
9. Ryan, T. A., Reuter, H. & Smith, S. J. Optical detection of a quantal presynaptic membrane turnover. *Nature* **388,** 478–482 (1997).
10. Mundy, D. I., Machleidt, T., Ying, Y. S., Anderson, R. G. & Bloom, G. S. Dual control of caveolar membrane traffic by microtubules and the actin cytoskeleton. *J. Cell Sci.* **115,** 4327–4339 (2002).
11. Drab, M. *et al.* Loss of caveolae, vascular dysfunction, and pulmonary defects in caveolin-1 gene-disrupted mice. *Science* **293,** 2449–2452 (2001).
12. Miesenbock, G., De Angelis, D. A. & Rothman, J. E. Visualizing secretion and synaptic transmission with pH-sensitive green fluorescent proteins. *Nature* **394,** 192–195 (1998).
13. Parton, R. G. Ultrastructural localization of gangliosides; GM1 is concentrated in caveolae. *J. Histochem. Cytochem.* **42,** 155–166 (1994).
14. Pelkmans, L., Kartenbeck, J. & Helenius, A. Caveolar endocytosis of simian virus 40 reveals a new two-step vesicular-transport pathway to the ER. *Nature Cell Biol.* **3,** 473–483 (2001).
15. Frolov, V. A., Lizunov, V. A., Dunina-Barkovskaya, A. Y., Samsonov, A. V. & Zimmerberg, J. Shape bistability of a membrane neck: a toggle switch to control vesicle content release. *Proc. Natl Acad. Sci. USA* **100,** 8698–8703 (2003).
16. Toomre, D., Steyer, J. A., Keller, P., Almers, W. & Simons, K. Fusion of constitutive membrane traffic with the cell surface observed by evanescent wave microscopy. *J. Cell Biol.* **149,** 33–40 (2000).
17. Parton, R. G., Joggerst, B. & Simons, K. Regulated internalization of caveolae. *J. Cell Biol.* **127,** 1199–1215 (1994).
18. Henley, J. R., Krueger, E. W., Oswald, B. J. & McNiven, M. A. Dynamin-mediated internalization of caveolae. *J. Cell Biol.* **141,** 85–99 (1998).
19. Minshall, R. D. *et al.* Endothelial cell-surface gp60 activates vesicle formation and trafficking via G_i-coupled *Src* kinase signalling pathway. *J. Cell Biol.* **150,** 1057–1070 (2000).
20. Sharma, D. K. *et al.* Selective stimulation of caveolar endocytosis by glycosphingolipids and cholesterol. *Mol. Biol. Cell* **15,** 3114–3122 (2004).
21. Salim, K. *et al.* Distinct specificity in the recognition of phosphoinositides by the pleckstrin homology domains of dynamin and Bruton's tyrosine kinase. *EMBO J.* **15,** 6241–6250 (1996).
22. Shajahan, A. N. *et al.* Role of Src-induced dynamin-2 phosphorylation in caveolae-mediated endocytosis in endothelial cells. *J. Biol. Chem.* **279,** 20392–20400 (2004).
23. Pelkmans, L. & Helenius, A. Insider information: What viruses tell us about endocytosis. *Curr. Opin. Cell Biol.* **15,** 414–422 (2003).

Supplementary Information is linked to the online version of the paper at www.nature.com/nature.

Acknowledgements We thank K. Anderson and S. Diez for help with TIR-FM, and M. Drab for *Cav1*$^{-/-}$ fibroblasts. D. Dorris, R. Günther, I. Baines and the Max Planck Institute for Molecular Cell Biology and Genetics are acknowledged for having made possible the kinome screen of endocytosis. We thank D. Meder, K. Simons, A. Helenius and Y. Kalaidzidis for discussions and critical reading of the manuscript. L.P. would like to thank A. Helenius for support. This work was supported by grants from The Max Planck Society 'RNAi interference' initiative and the Bunderministerium für Bildung und Forschung. L.P. is a Marie Curie Fellow.

Author Information Reprints and permissions information is available at npg.nature.com/reprintsandpermissions. The authors declare no competing financial interests. Correspondence and requests for materials should be addressed to L.P. (pelkmans@mpi-cbg.de).